Pergamon

Int. J. Heat Mass Transfer. Vol. 41, Nos 8–9, pp. 1075–1086, 1998

Printed in Great Britain
0017–9310/98 $19.00+0.00

PII: S0017–9310(97)00174–9

Analytical model of induced electric current from a free convection loop placed in a transverse magnetic field

N. GHADDAR

American University of Beirut, Faculty of Engineering and Architecture, 850 Third Ave, New York, NY 10022, U.S.A.

(*Received* 28 *October* 1996 *and in final form* 4 *June* 1997)

Abstract—The hydrodynamics characteristics of buoyancy-driven convection loop containing an electrically-conducting fluid in a transverse magnetic field is investigated analytically using one-dimensional model. The lower portion of the loop is heated and the upper portion is cooled, both isothermally, while the middle portion is insulated. The model was based on the use of Hartmann plane Poiseuille flow solution for estimating loop shear stress. The study covers the range of Grashof number, Gr, from 10^2 to 10^6, the Hartmann number, Ha, from 0 to 20, and the Prandtl number, Pr, from 0.02 to 7. The proposed closed form analytical solution of the magnetohydrodynamic generator predicts the flow velocity and the induced current in terms of the flow and geometric parameters. It is shown also that at low Prandtl numbers, $Pr \ll 1$, there exist an optimal Hartmann number, Ha_{opt}, that maximises the induced electric current and Ha_{opt} depends weakly on Grashof number. The existence of an optimal Hartmann number is significant in optimising the loop efficiency of conversion from thermal to electrical energy in presence of a transverse magnetic field. © 1997 Elsevier Science Ltd.

1. INTRODUCTION

Natural convection in closed loops plays an important role in the design of thermal energy systems which are characterised by at least one heat source and some heat sinks positioned at some height about the source. When a transverse magnetic field is applied on an electrically conducting fluid in the loop, convective motion is damped and an electric current is induced. The interest in such problem has two aspects. The first aspect lies in industrial processes or energy systems that require control of flow destabilisation or prohibition of motion. The second interest lies in the possible use of the system for electricity generation. In the power industry, among methods of generating electric power is one in which electric energy is extracted directly from a moving conducting fluid in a magnetic field. The difference here is that the motion is produced by thermosyphonic motion of the conducting fluid.

Several aspects of convective motion characteristics of single-phase closed loop thermosyphon have been much discussed in literature particularly in relation to stability characteristics, Creveling *et al.* [1] studied the dynamics of the thermosyphonic flow in single circular loop system exhibiting typical nonlinear effects using one-dimensional analysis and verifying his model with experimental observations. Recently, Erhard *et al.* [2] and Davis and Roppo [3] investigated double-loop systems where two circular loops were coupled by a heat exchanger for different coupling locations. Their experiments and mathematical models confirmed the existence of a subcritical parameter range that alternatively exhibit steady as well as time dependent behaviour. Related work reported in literature is for forced convection. The first MHD channel flow was first investigated in 1930 by Hartmann [4], who considered plane Poiseuille flow with a transverse magnetic field. No work has been reported so far on the effect of a transverse magnetic field on thermosyphonic motion.

Closed form solutions are usually of great importance in magnetohydrodynamic flows because they can be used to check numerical solutions and to develop understanding into the relative influence of the physical parameters involved in the problem. This can be accomplished by making simplifications whereby the governing equations reduce to a form that can be solved analytically. In this work, an analytical one-dimensional solution based on parallel flow approximation of the loop convection in presence of a transverse magnetic field is developed. The fluid is assumed incompressible, electrically conducting and fully-developed with no applied electric field. The model is based on the use of Hartmann plane Poiseuille flow solution for estimating loop shear stress. The range of validity of the approximate solution is discussed. The optimisation of the system parameters for maximisation of the induced electric current is investigated.

2. PROBLEM STATEMENT

The essential features of the thermosyphonic closed loop are shown in Fig. 1. The loop has a height $2L$,

NOMENCLATURE

A	defined in equation (8a)
A'	$A/\Delta T$
B	defined in equation (8b)
B'	$B/\Delta T$
B_0	magnetic field strength
C	specific heat
$2d$	channel width
Ec	Eckert number, $Vo^2/C\Delta T$
f	friction factor for laminar channel flow
g	gravitational acceleration
Gr	Grashof number, $g\beta\Delta Td^3/\nu^2$
h	heat transfer coefficient in the loop channel
Ha	Hartmann number, $B_0 d(\sigma/\rho_0\nu)^{1/2}$
j	induced electric current
K	defined in equation (12b)
$2L$	vertical height of the loop
$2l$	height of the insulated region
m	defined in equation (6)
Nu	Nusselt number, hd/k
p	pressure
Pr	Prandtl number, ν/α
Q_L	heat transfer rate carried by the loop
Re	Reynolds number, $V_0 d/\nu$
S	parameter defined in equation 12(c)
t	time
T	temperature
V_0	bulk induced velocity in the loop
(x, y, z)	Cartesian co-ordinates.

Greek symbols

α	thermal diffusivity
β	thermal expansion coefficient
ΔT	temperature difference between hot and cold segments, $T_H - T_C$
Γ	heat transfer parameter defined in equation (20)
θ	dimensionless temperature, $(T-T_c)/(T_H-T_C)$
μ	fluid viscosity
ν	kinematic viscosity of the fluid
ρ_0	density of the fluid
σ	electrical conductivity
τ	shear stress in the channel.

Subscripts

b	bulk values
c	cold
f	friction factor model
H	hot.

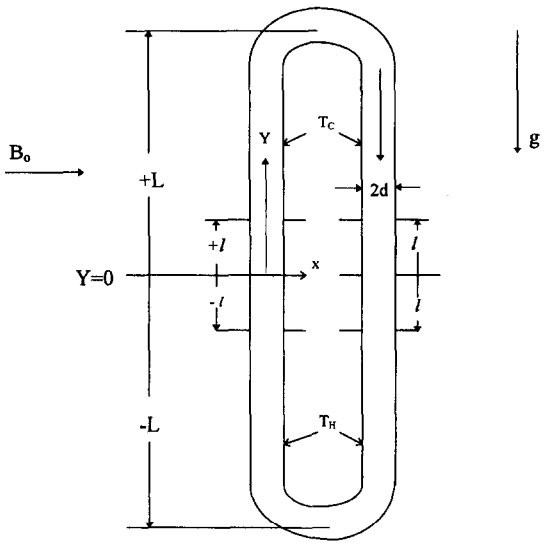

Fig. 1. The essential features of the thermosyphonic closed loop.

an internal channel half-width of d. the upper and lower connecting portions of the vertical channel are semi-circular. The boussinesq fluid contained in the loop is *electrically conducting* with an electrical conductivity σ, and a coefficient of thermal expansion β. Examples of electrically conducting fluids are mercury, sodium, sea water or ionised gases. The magnetic field B_0 is applied perpendicular to gravity in x-direction. The thermophysical properties of the fluid at a reference temperature T_C are assumed to be constant except for the density which is related to temperature according to $\rho = \rho_0(1-\beta(T-T_C))$. The lower half of the loop wall is isothermally heated to T_H and the upper half of the loop wall is isothermally cooled to T_C, which is taken as the reference temperature. The central region of the loop of length $2l$ is insulated.

Assuming the channel width of the loop to be much smaller than its length L, i.e. $2d \ll L$, the one dimensional model of the flow and heat transfer can be used with sufficient accuracy [2]. To simplify the coordinate system, end effects of the top and bottom parts of the loop are neglected and the origin of the y-axis is placed in the midpoint of the left segment of the loop, parallel to the flow direction as it moves against gravity and then with gravity. The flow is steady and is assumed fully-developed such that the physical flow variables are independent of the axial coordinates. These variables are the cross-sectionally averaged velocity V_0 and the associated wall shear

stress. Axial heat conduction and viscous heating are neglected and the steady conservation equations of momentum and energy for the fully-developed hydrodynamic flow are written in terms of V_0 and bulk temperature T_b:

momentum

$$0 = -\frac{\partial p}{\partial y} - \rho g - \sigma V_0 B_0^2 - \frac{\tau}{d} \tag{1}$$

energy in the isothermal regions $-2L+l \leqslant y \leqslant -1$ and $l \leqslant y \leqslant 2L-l$

$$\rho C\left[V_0 \frac{\partial T_b}{\partial y}\right] = \frac{h}{2d}\{T_w - T_b(y)\} + \sigma V_0^2 B_0^2 \tag{2}$$

and energy in the insulated regions $-l \leqslant y \leqslant +1$ and $2L-l \leqslant y \geqslant -2L+1$

$$\rho C\left[V_0 \frac{\partial T_b}{\partial y}\right] = \sigma V_0^2 B_0^2 \tag{3}$$

where h is the convection heat transfer coefficient in the channel, $\sigma B_0^2 V_0^2$ is the Joulean heating term, and T_w is the loop wall temperature in the isothermal regions defined by:

$$T_w = T_H \quad \text{for } -2L+l \leqslant y \quad \text{and} \quad y \leqslant -1 \tag{4a}$$

$$T_w = T_C \quad \text{for } l \leqslant y \leqslant 2L-l. \tag{4b}$$

Equations (1)–(3) are solved for steady-state conditions in the next section.

3. ANALYTICAL STEADY-STATE SOLUTION

3.1. *Hartmann–plane Poiseuille flow model*

The steady-state conditions fully-developed flow indicate that the mass flux ρV_0 is constant along the loop. So the energy transfer equation (3a) can be solved for temperature distribution along the loop in terms of V_0:

$$T_b = \begin{cases} Ae^{-my} + T_H + \dfrac{2\sigma B_0^2 V_0^2 d}{h} \\ \qquad \text{for } -2L+l \leqslant y \leqslant -1 \\ Be^{-my} + T_c + \dfrac{2\sigma B_0^2 V_0^2 d}{h} \\ \qquad \text{for } +l \leqslant y \leqslant 2L-l \end{cases} \tag{5a,b}$$

where the parameter m is given by:

$$m = h/(2\rho C V_0 d). \tag{6}$$

Solution of equation (3b) in the insulated sections gives a linearly increasing bulk temperature due to Joulean heating in each segment. Therefore, imposing the continuity condition of bulk temperature in those segments:

$$T_b(l) = T_b(-l) + 2\sigma B_0^2 V_0 l/\rho C \tag{7a}$$

$$T_b(-2L+l) = T_b(2L-l) + 2\sigma B_0^2 V_0 l/\rho C \tag{7b}$$

leads to expressions for the parameters A and B of equation (5) given by:

$$A = (T_H - T_C)\frac{[1-e^{-2m(L-l)}]}{[e^{-m(2L-3l)} - e^{m(2L-l)}]} - \frac{2\sigma B_0^2 V_0 l}{\rho C}\frac{[1+e^{-2m(L-l)}]}{[e^{-m(2L-3l)} - e^{m(2L-l)}]} \tag{8a}$$

$$B = Ae^{2ml} + \left[(T_H - T_C) + \frac{2\sigma B_0^2 V_0 l}{\rho C}\right]e^{ml}. \tag{8b}$$

In this development it is assumed that h is constant throughout the loop. This assumption is valid for small values of V_0. for moderate values of V_0 the heat transfer is generally improved with h varying as $h \propto V_0^{1/3}$ in the laminar flow regime [2].

Now the momentum equation (2) integrated around the loop gives:

$$4\frac{\tau L}{d} + 4\sigma\rho_0 V_0 B_0^2 L = \rho_0 g\beta\left[-\int_{-2L}^{-2L+l}(T-T_0)\,dy - \int_{-2L+l}^{-L}(T-T_0)\,dy + \int_{-L}^{-l}(T-T_0)\,dy + \int_{-l}^{l}(T-T_0)\,dy + \int_{l}^{L}(T-T_0)\,dy - \int_{L}^{2L-l}(T-T_0)\,dy - \int_{2L-l}^{2L}(T-T_0)\,dy\right] \tag{9}$$

which shows balance between buoyancy, Lorentz force and friction where pressure variations in the loop are only due to gravity. The negative and positive signs of the buoyant terms is related to gravity direction where it is positive for the upward going flow and negative for the downward going flow and in each integral segment the respective bulk temperature is used depending if it is an isothermal region or an insulated region. The flow in the channel is assumed fully developed and the solution of Hartmann [4] for MHD plane Poiseuille flow with a transverse magnetic field is used to correlate the walls shear stress force to the mean flow velocity V_0 by:

$$\tau = \frac{\mu V_0}{d} Ha^2 \frac{\tanh(Ha)}{Ha - \tanh(Ha)} \tag{10}$$

where Ha is the Hartmann number is defined by $Ha = B_0 d(\sigma/\rho_0 \nu)^{1/2}$. The square of the Hartmann number represents the ratio of the Lorentz force from the induced current to the viscous forces. For comparison, the quantity $(\sigma/\rho_0\nu)^{1/2}$ for mercury ($Pr \approx 0.02$) is about 2.7×10^5 while for sea water ($Pr \approx 7$) it is about 65. Using the value of τ in (10) and evaluating the integral of the buoyancy term using the temperature distribution obtained in equation (5), reduces equation (8) to the following:

$$\frac{4\mu V_0 Ha^2 \tanh Ha}{d^2(Ha-\tanh Ha)} + 4\sigma\rho_0 V_0 B_0^2 = \rho g\beta\left[\frac{A}{mL}(2e^{mL}-e^{m(2L-l)}-e^{ml}) + \frac{B}{mL}(e^{-ml}+e^{-m(2L-l)}-2e^{-mL})\right] + \rho g\beta\left[\frac{l}{L}(A(e^{ml}-e^{m(2L-l)})-B(e^{-ml}+e^{-m(2L-l)})\right]. \quad (11)$$

Equation (11) gives a correlation between the induced flow velocity V_0 and the other flow and geometric parameters in the system. Equation (11) can then be reduced to a non-dimensional form in the following correlation:

$$Gr = \frac{4ReHa^2\left[1+\dfrac{\tanh Ha}{Ha-\tanh Ha}\right]}{\dfrac{2l}{L}[S]+\dfrac{4RePr[K]}{(L/d)Nu}} \quad (12a)$$

where K is defined as

$$K = \tfrac{1}{2}[A'(2e^{mL}-e^{ml}-e^{m(2L-l)}) + B'(e^{-ml}+e^{-m(2L-l)}-2e^{-mL})] \quad (12b)$$

S is defined as

$$S = \tfrac{1}{2}[A'(e^{ml}-e^{m(2L-l)})+B'(e^{-ml}-e^{-m(2L-l)})] \quad (12c)$$

and A' and B' are dimensionless terms obtained from equation (8) and given by

$$A' = \frac{[1-e^{-2m(L-l)}]}{[e^{-m(2L-3l)}-e^{m(2L-l)}]} - \frac{2Ha^2 Ec(l/d)}{Re}\frac{[1-e^{-2m(L-l)}]}{[e^{-m(2L-3l)}-e^{m(2L-l)}]} \quad (12d)$$

$$B' = A'e^{2ml}+\left[1+\frac{2Ha^2 Ec(l/d)}{Re}\right]e^{ml}. \quad (12e)$$

The dimensionless parameters appearing in equation (12) are defined as: Re is the Reynolds number, $Re = V_0 d/\nu$, Gr is the Grashof number, $Gr = g\beta\Delta T d^3/\nu^2$, where ΔT is the temperature difference between hot and cold walls, $\Delta T = T_H - T_C$, Ha is the Hartmann number, Nu is the Nusselt number, $Nu = hd/k$, Ec is the Eckert number, $Ec = Vo^2/C\Delta T$ and Pr is the Prandtl number, $Pr = \nu/\alpha$. The dimensionless parameters mL and ml can also be expressed in terms of the flow and geometric parameters of the system, where $mL = (Nu/2RePr)(L/d)$ and $ml = (Nu/2RePr)(l/d)$. Note that in the solution there is no restriction on the relative size, l/L, of the insulated region to the isothermal regions. The general solution obtained in equations (12) is valid for all values of Prandtl numbers, Hartmann numbers and Grashof numbers in the laminar range with $d \ll L$ to insure parallel flow assumptions.

The parameters K and S of equation (12) are bounded between zero and one, i.e. $0 \leqslant K \leqslant 1$ and $0 \leqslant S \leqslant 1$ for all values of flow parameters as can be seen from Fig. 2(a) and (b), respectively. At high Prandtl number and Reynolds number flow, $K \to 0$, but the term $[K]PrRe/Nu(L/d)$ in the dominator of equation (12a) remains significant. At low Prandtl numbers ($Pr \ll 1$) and low to moderate Reynolds numbers, both parameters K and S approach unity ($K \to 1$ and $S \to 1$) which simplifies equation (12a) to get an explicit correlation of the dependent parameter Re as:

$$Re = \frac{2(l/L)Gr}{4Ha^2+\dfrac{4Ha^2\tanh Ha}{Ha-\tanh Ha}-\dfrac{4PrGr}{Nu(L/d)}} \quad \text{for } Pr \ll 1. \quad (13)$$

The induced electric current j in the direction perpendicular to the plane of the magnetic field and flow velocity, can then be written as:

$$j = \sigma(V_0\hat{y}\times B_0\hat{x}) = ReHa\left(\frac{\nu}{d^2}\sqrt{\sigma\mu}\right)\hat{z} \quad (14)$$

and the induced electric current for low Prandtl numbers $Pr \ll 1$ is then given by

$$j = \left(\frac{\nu}{d^2}\sqrt{\sigma\mu}\right)\left[\frac{2(l/L)GrHa}{4Ha^2+\dfrac{4Ha^2\tanh Ha}{Ha-\tanh Ha}-\dfrac{4PrGr}{Nu(L/d)}}\right] \quad Pr \ll 1. \quad (15)$$

In the discussion of the flow behaviour associated with the proposed one-dimensional solution, we can show that the physics of the flow is perfectly described with both flow and geometric parameters taken into consideration.

3.2. *Friction factor model solution and the limiting case of zero Hartmann number*

The special case of $Ha = 0$ cannot be derived directly from the developed solutions in equation (12)–(15) because of the way the shear stress is defined. For comparison purposes of physical results, the $Ha = 0$ case is solved in this section. The governing equations of momentum and energy transfer (1)–(4) of the free-convection loop are solved now using the same procedure of the previous Section 3.1, but with using the friction factor in defining the shear stress rather than the Hartmann–Poiseuille flow model of shear.

The bulk temperature distribution of the friction factor model in the domain is exactly the same as that obtained in equation (5), but with removing the heat

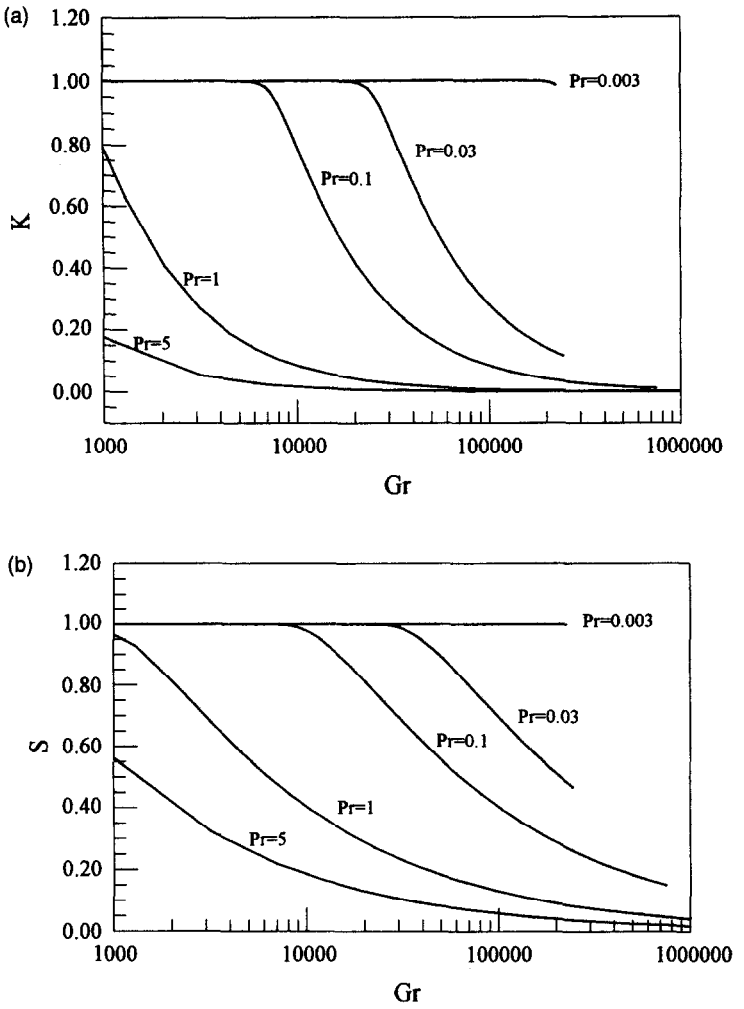

Fig. 2. A plot of the K parameter and the S parameter in (a) and (b), respectively, as a function of Grashof number for $L/d = 20$, $l/L = 0.1$, $Ha = 5$ and $Nu = 1.86$ at various Prandtl numbers.

source term due to the induced current by B_0 which even in Hartmann–Poiseuille model has been eventually been neglected. The difference in the solution for the induced velocity in the friction factor model comes from the handling of the shear stress force term in equation (9) which will be expressed as $\tau = f\rho V_0^2/2$, where f is the friction factor correlated for laminar flow fully developed flow in a plane channel by $f = 24/Re_{Dh}$, where Re_{Dh} is based on the hydraulic diameter of the channel. Substituting $\tau = f\rho V_0^2/2$ into equation (9) and performing the necessary algebra will lead to a correlation for the flow parameters as:

$$Gr = \frac{Re(12+4Ha^2)}{\frac{2l}{L}[S] + \frac{4RePr[K]}{(L/d)Nu}} \quad \text{'friction factor model'} \tag{16}$$

which applies to natural convection loop. At very low Prandtl number ($K \to 1$ and $S \to 1$), the Reynolds number can explicitly be obtained as:

$$Re_f = \frac{2(l/L)Gr}{12+4Ha^2 - \frac{4PrGr}{Nu(L/d)}}$$

'friction factor model' for $Pr \ll 1$ (17a)

where Re_f is based on friction factor model. The induced electric current for low Prandtl numbers $Pr \ll 1$ is then given by:

$$j_f = \left(\frac{\nu}{d_H^2}\sqrt{\sigma\mu}\right)\left[\frac{2(l/L)GrHa}{12+4Ha^2 - \frac{4PrGr}{Nu(L/d_H)}}\right]$$

'friction factor model' for $Pr \ll 1$ (17b)

where j_f represent the induced electric current based on the friction factor model. The free convection solution obtained in (16) and (17) for the case of zero magnetic field strength, $Ha = 0$, represents the upper bound on values of the induced velocity at various Grashof numbers for the Hartmann–Poiseuille model.

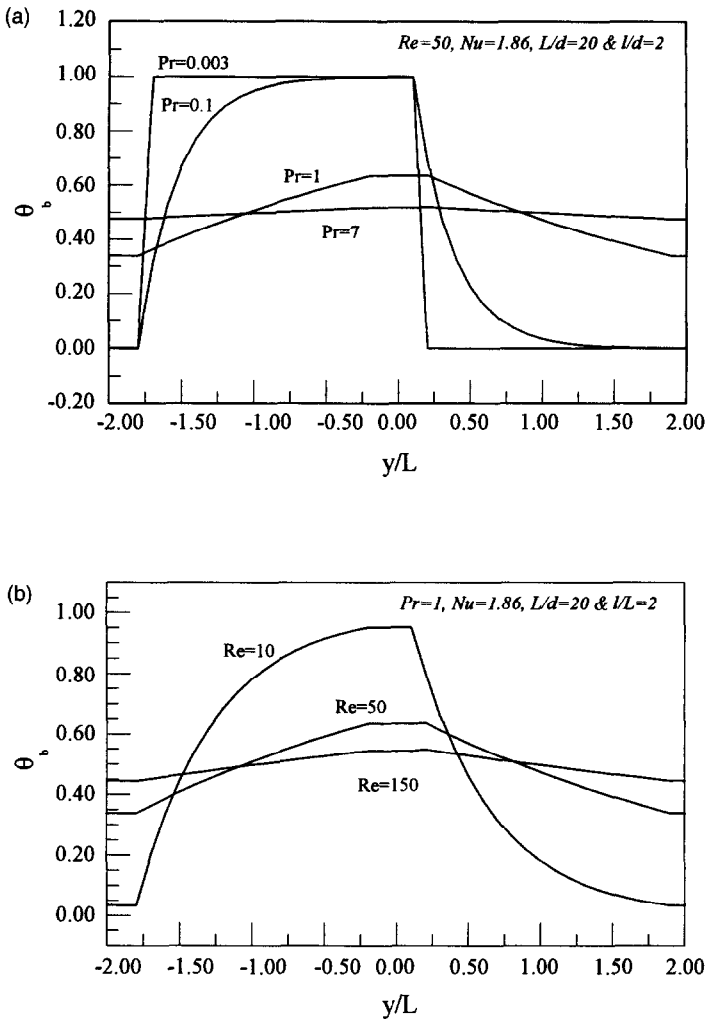

Fig. 3. The dimensionless bulk temperature distribution, $\theta_b = (T_b - T_c)/(T_H - T_c)$ along the loop for $L/d = 20$, $l/L = 0.1$, $Ha = 1$ for (a) $Re = 50$, $Pr = 0.02$, 1 and 5, and for (b) $Pr = 1$ and $Re = 10$, 50 and 150.

4. RESULTS AND DISCUSSION

4.1. *Hartmann–Poiseuille flow model results*

The one-dimension proposed Hartmann–Poiseuille solution of the stable laminar steady flow in the thermosyphonic loop is presented in this section. The Eckert number Ec is taken as zero throughout the analysis since expected induced current is very small to cause significant warming of the fluid in the loop. Figure 3 shows the dimensionless bulk temperature distribution, $\theta_b = (T_b - T_c)/(T_H - T_c)$ along the loop at $L/d = 10$, $l/d = 1$, $Ha = 5$ for (a) $Re = 50$, for various Prandtl numbers and for (b) $Pr = 1$ for various values of Reynolds numbers. The maximum temperature difference $(T_b - T_w)$, and hence maximum rates of heat transfer occur as the upward moving hot fluid enters the cold segment at $y = l$ and as the down moving cooled fluid is entering the hot section at $y = (-2L + l)$ at the end of the insulated segment.

Figure 4 shows the variation of Reynolds number, Re, as a function of Grashof number, Gr, as obtained in equation (12) at $Nu = 1.86$, $L/d = 20$, $l/d = 2$ and various values of Hartmann number, Ha, for: (a) $Pr = 0.02$; (b) $Pr = 1$; and (c) $Pr = 7$. It is clear that as the magnetic field strength is increased, a higher driving buoyancy force is needed to attain the same circulation velocity. In the limit as Hartmann number becomes high, the flow Reynolds number at fixed Grashof number follows an $(Ha)^{-2}$ power law. At zero magnetic field, $Ha = 0$, the friction factor model solution obtained in equation (16) is also seen in Fig. 4 and the induced velocity is the highest at fixed Grashof number and non-zero Hartmann numbers.

The effect of Prandtl number on the flow is shown

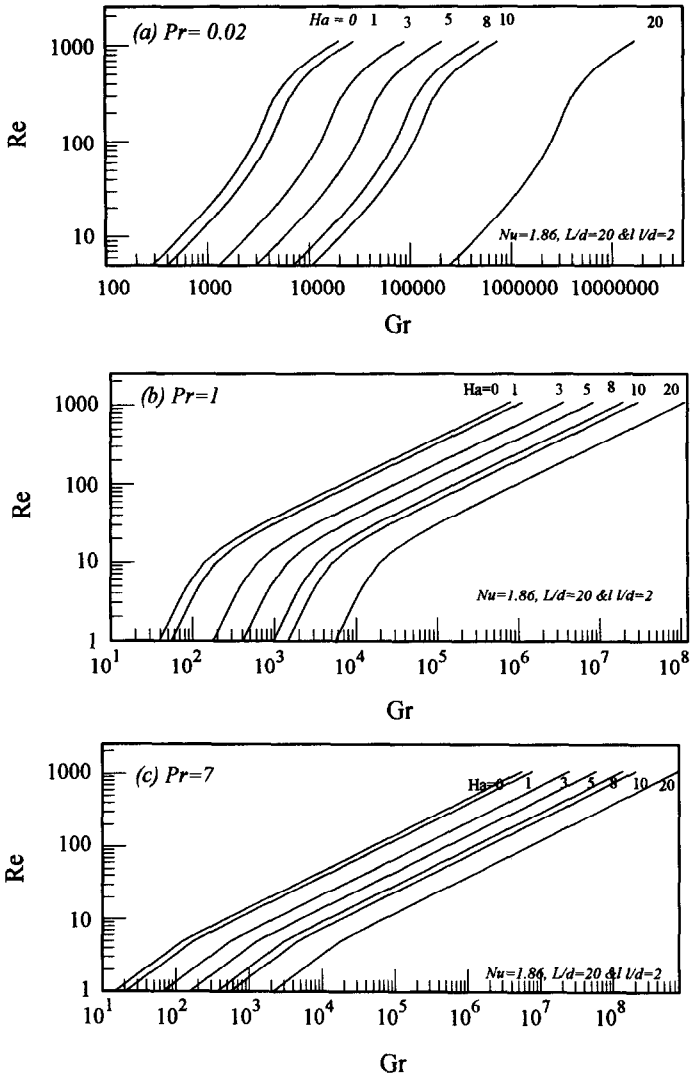

Fig. 4. The variation of Reynolds number, Re, as a function of Grashof number, Gr, at $Nu = 1.86$, $L/d = 20$, $l/d = 2$ and various values of Hartmann number at (a) $Pr = 1$, (b) $Pr = 7$, and (c) $Pr = 0.02$.

in Fig. 5, where Reynolds number is plotted against Grashof number for $L/d = 20$, $l/d = 2$, $Ha = 5$ and various values of $Pr = 0.02$, 0.2, 1 and 7. As Re becomes larger than 1000, the flow becomes strongly dependent on Pr. The smaller the Prandtl number, the higher is the required Grashof number (buoyancy term) to maintain the same flow rate. In the low Grashof and Reynolds numbers range, the system behaviour is different and a lower Grashof number is needed for small Pr-fluid than a high-Pr fluid to maintain a given flow.

The product of the Reynolds and Hartmann numbers if related to the induced current directly by $ReHa = jd^2/\{\nu(\sigma\mu)^{1/2}\}$. Figure 6 shows the dimensionless induced electric current parameter $jd^2/\{\nu(\sigma\mu)^{1/2}\}$ as a function of Grashof number for: (a) $Pr = 0.02$; (b) $Pr = 1$; and (c) $Pr = 7$ at $L/d = 20$, $l/d = 2$ and $Nu = 1.86$. At fixed Hartmann number, the induced current increases as the Grashof number is increased due to increased buoyancy force which directly affect the flow.

At low Prandtl numbers, the induced electric current parameter $jd^2/\{\nu(\sigma\mu)^{1/2}\}$ is explicitly correlated to Grashof and Hartmann number [see equation (15)] and it is shown in Fig. 7 as a function of Hartmann number at various Grashof numbers. It is obvious that there is an optimal Hartmann number that maximises the induced electric current. The logarithmic scale used in Fig. 8 smoothes out the sharp peaks of induced electric current where for example at $Gr = 10{,}000$, the peak value of $ReHa$ is equal to 754.2 at $Ha = 1.54977$ compared to 443.8 at $Ha = 0.5$ and $ReHa = 442.86$ at $Ha = 5$. So about 70% increase in induced current at $H_{opt} = 1.54977$ over values observed at $Ha = 0.5$ and 5. The optimal Hartmann number is found by differentiating equation (15) with

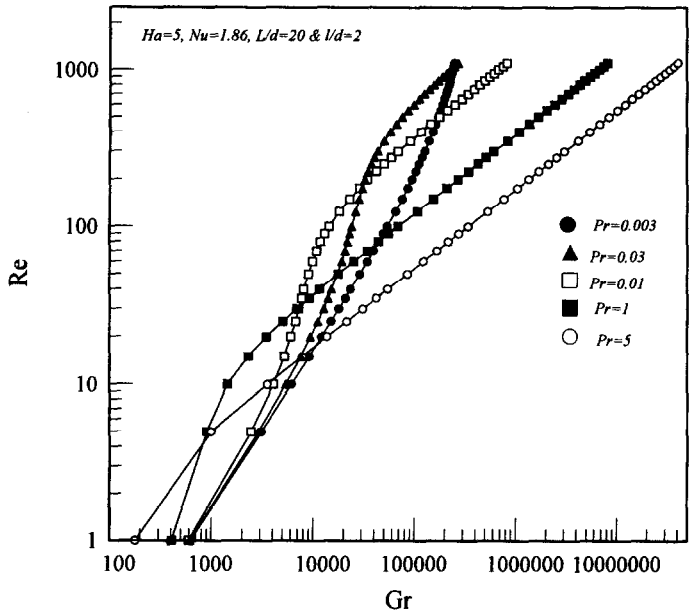

Fig. 5. Reynolds number is plotted against Grashof number for $L/d = 20$, $l/d = 2$, $Ha = 5$ and various values of $Pr = 0.003$, 0.03, 0.1, 1 and 5.

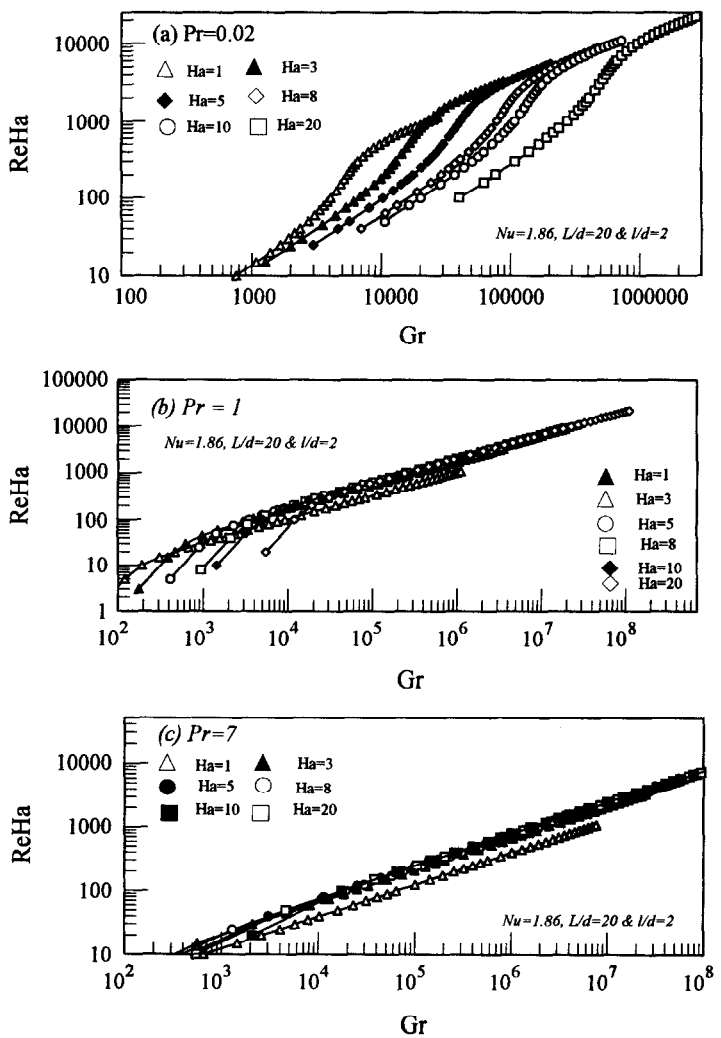

Fig. 6. The dimensionless induced electric current parameter $jd^2/\{v(\sigma\mu)^{1/2}\}$ as a function of Grashof number for (a) $Pr = 0.02$, (b) $Pr = 1$ and (c) $Pr = 7$ at $L/d = 20$, $l/d = 2$ and $Nu = 1.86$.

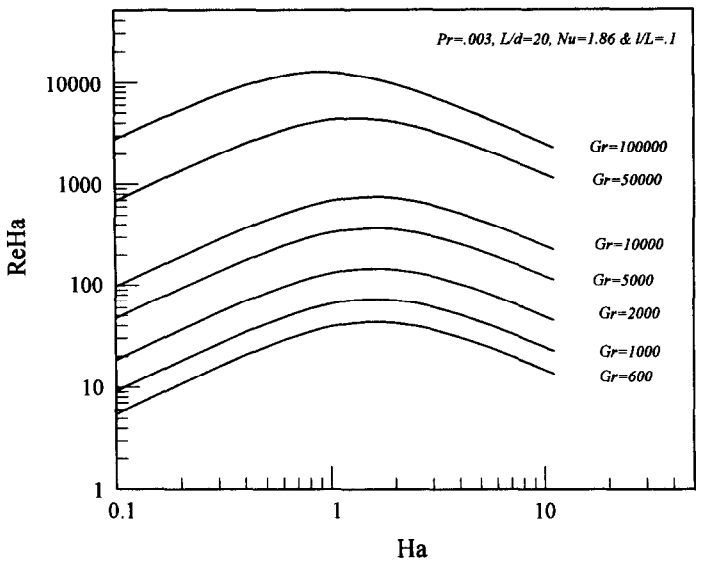

Fig. 7. The dimensionless induced electric current parameter $jd^2/\{\nu(\sigma\mu)^{1/2}\}$ as a function of Hartmann number at various Grashof numbers for $Pr = 0.003$, $L/d = 20$, $l/d = 2$ and $Nu = 1.86$.

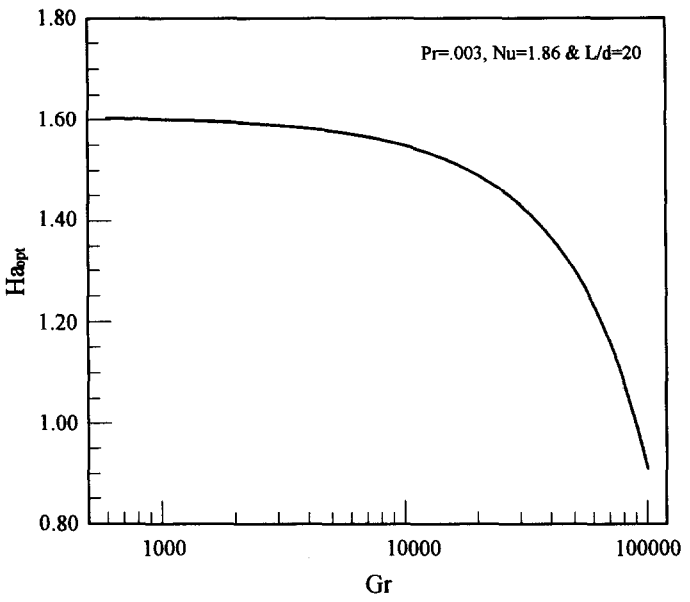

Fig. 8. The optimal Hartmann number is plotted against Grashof number at $Pr = 0.003$.

respect to Ha and equating the result to zero which gives after some algebraic manipulations the following relation for Ha_{opt}:

$$0 = -4Ha_{opt}^4 NuL/d - GrHa_{opt}^2 Pr - 4Ha_{opt}^4 Nu(L/d)\sec h^2(Ha_{opt}) + 2GrHa_{opt}Pr\tanh(Ha_{opt}) - GrPr\tanh^2(Ha_{opt}) + 8Ha_{opt}^3 Nu(L/d)\tanh(Ha_{opt}). \quad (18)$$

The roots of equation (18) for optimal Hartmann number can then be found for given values of Gr, Pr, Nu and L/d. The optimal Hartmann number that maximises the induced current for low Prandtl numbers is plotted in Fig. 8 as a function of the Grashof number for the case of $Nu = 1.86$, $L/d = 20$ and $Pr = 0.003$. The optimal Hartmann number decreases as Grashof number is increased. It is interesting that the maximum induced current occurs at quite a low magnetic field strength ($Ha < 2$). Hypothetically, in the limit as $Gr \to \infty$, the optimal Hartmann number, approaches zero, $H_{opt} \to 0$.

In the laminar range of the induced steady flow, the presence of H_{opt} is very significant in terms of improving the system efficiency of conversion from thermal to electrical in the system in presence of a lower strength magnetic field. The heat transfer carried from the heat source (hot lower portion of the

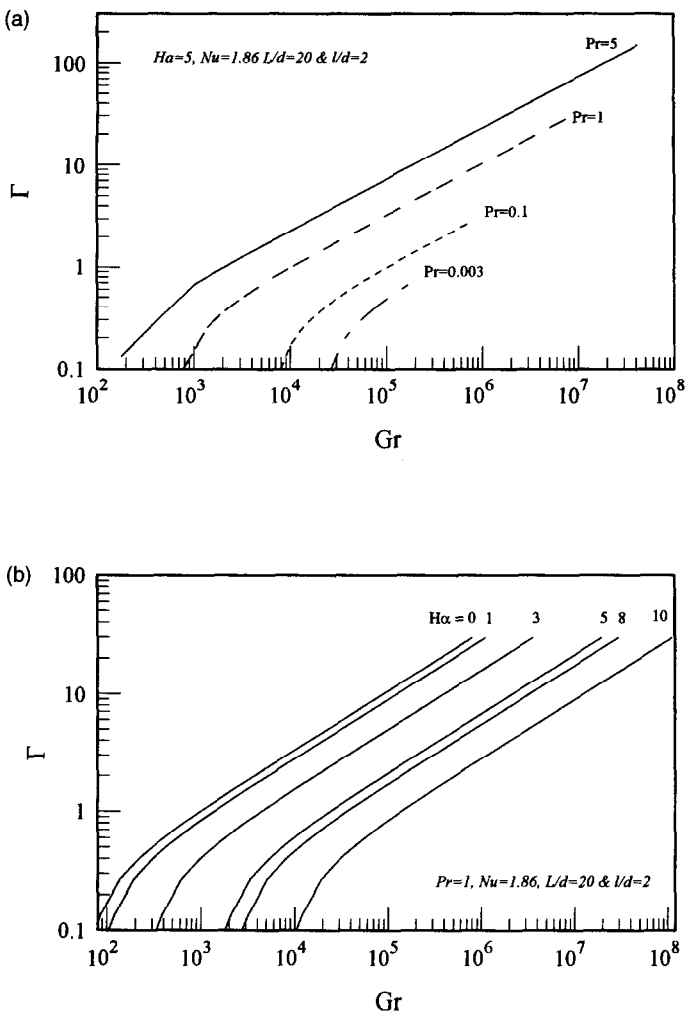

Fig. 9. The heat transfer parameter, Γ, plotted as a function of *Gr* number for (a) various Prandtl numbers and for (b) different values of Hartmann number at $L/d = 20$, $l/d = 0.1$, $Nu = 1.86$.

loop) to the heat sink (cold upper portion of the loop) is given by:

$$Q_L = 2h\int_l^{2L-l} (T_b(y) - T_c)\,dy. \tag{19}$$

Using the expression for $T_b(y)$ of equation (5b) and integrating equation (19) gives the rate of heat loss from the upper cold portion of the loop in dimensionless form as:

$$\Gamma = \frac{Q_L}{2LH\Delta T} = \left(\frac{B' RePr}{Nu(L/d)}[e^{-m(2L-l)} - e^{-ml}] + \frac{4Ha^2 EcPr}{Nu}\right) \tag{20}$$

where B' was defined earlier as $B/\Delta T$ and B is given in equation (7b). The heat transfer parameter, Γ, defined in equation (20) is a function of all the system parameters: *Pr*, *Nu*, L/d, l/d and *Re*, where *Re* depends on *Gr* and *Ha*. In Fig. 9, the heat transfer parameter, Γ, is plotted as a function of *Gr* number at $L/d = 20$, $l/d = 2$, $Nu = 1.86$, $Ec = 0$ for different values of (a) Prandtl numbers at $Ha = 1$ and (b) Hartmann numbers at $Pr = 1$. As Prandtl number is increased the heat transfer parameter Γ increases at fixed Grashof number. The rate of heat transfer in presence of a magnetic field decreases with increased *Ha*, at fixed *Gr*, unlike the induced current dependence.

4.2. *Comparison between the Hartmann–Poiseuille and the friction factor models*

The MHD Hartmann–Poiseuille model for the free convection loop would represent the system behaviour more accurately than the friction factor model for large Hartmann number flows because it takes into account the changes in velocity gradients at the wall surface due to the presence of the magnetic field. This effect of the magnetic field on the shear stress is not

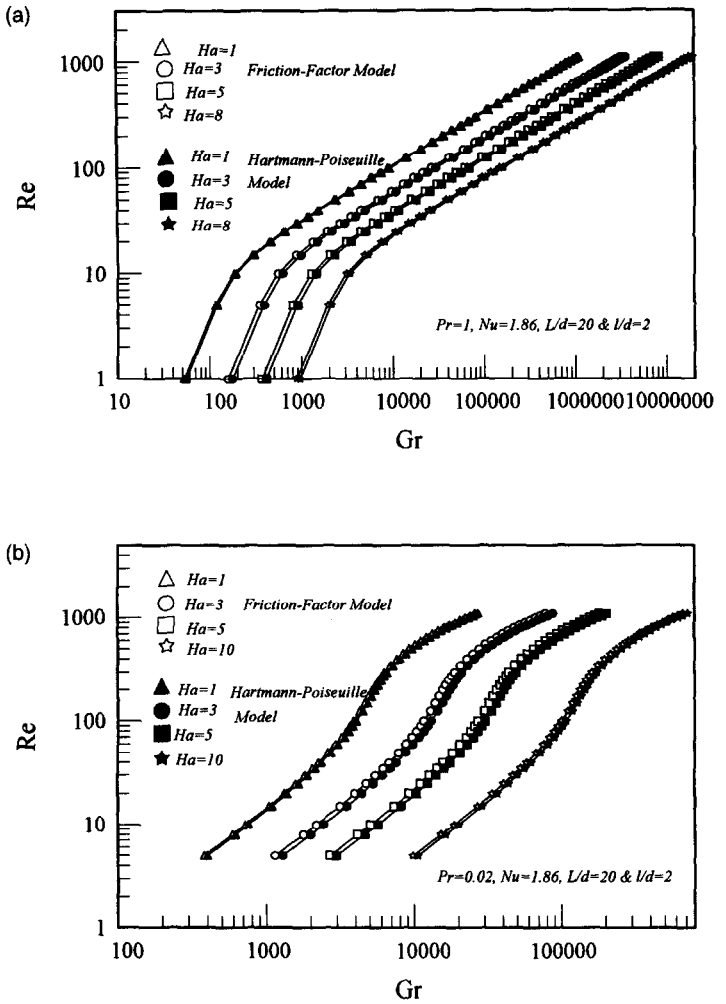

Fig. 10. The variation of Reynolds number with Grashof number in both models at various Hartmann numbers at (a) $Pr = 1$ and (b) $Pr = 0.02$ for $Nu = 1.86$, $L/d = 20$ and $l/L = 0.1$.

significant at low Hartmann numbers [5]. Figure 10 shows the variation of Reynolds number with Grashof number in both models at various Hartmann numbers at (a) $Pr = 1$ and (b) $Pr = 0.02$ for $Nu = 1.86$, $L/d = 20$ and $l/d = 2$. Both models give similar result for the induced flow Reynolds number at low Ha, but as Hartmann is increased the percentage difference in the solution reach values not more than 5% for $Ha < 20$. Generally the error difference is small at low Hartmann and also at high Reynold and Grashof numbers with intermediate values of Ha.

The friction factor model has the advantage of giving a simpler expression for the induced current as a function of Hartmann number and the other system parameters at low Prandtl numbers [compare equations (15) and (17b)]. Actually using the expression for j_f given in equation (17b), we can find a closed form relation for the optimal Hartmann number for maximum induced current as a function of the system parameters. This is done by differentiating equation (17b) with respect to Ha and equating $\partial j_f/\partial Ha$ to zero which gives an expression for H_{opt} as:

$$(Ha_{opt})_f = \sqrt{3 - \frac{GrPr}{Nu(L/d)}} \quad \text{for } Pr \ll 1 \qquad (21)$$

where subscript f refers to the friction factor model. A comparison is now made between the present model and the friction factor model. Figure 11 shows a plot of optimal Hartmann number vs Grashof number using both the friction factor model and the Hartmann–Poiseuille model. The friction factor model overpredicts Ha_{opt} by 7–9% as compared to the more accurate Hartmann–Poiseuille flow model.

5. CONCLUSIONS

A theoretical analysis was carried out with one-dimensional approach to derive the hydrodynamic model of buoyancy-driven electrically-conducting

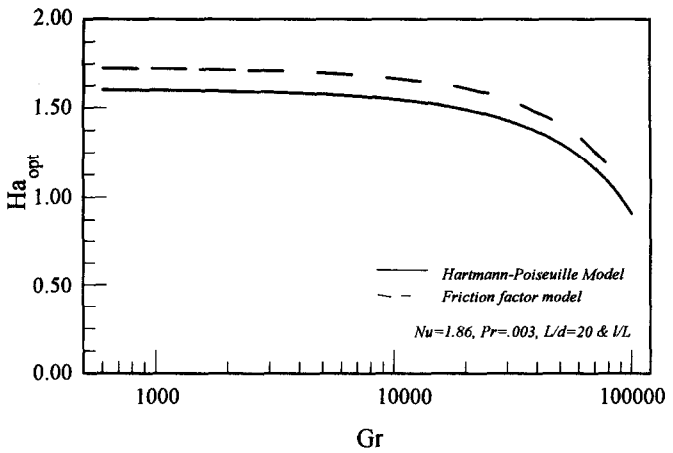

Fig. 11. A plot of optimal Hartmann number vs Grashof number using both the friction factor model and the Hartmann–Poiseuille model.

fluid in a vertical loop placed in a transverse magnetic field. The closed form solution of the flow velocity is used to predict the induced electric current of the system. According to the solution there exist an optimal strength of the magnetic field that depends on the system flow and geometric parameters to maximise the induced electric current. At high Grashof number only a low strength magnetic field is required to get a significant induced electric current. Future work will address the conversion efficiency of thermal to electrical energy of the described magneto hydrodynamic generator and will include experimental verification of the results.

Acknowledgements—The author greatly acknowledges the support of the University Research Board of the American University of Beirut to visit MIT Mechanical Engineering Department during the summer of 1995. The help of the research assistant Shawki Fattal is also acknowledged.

REFERENCES

1. Creveling, H. F., De Paz, J. F., Baladi, J. Y. and Schoenhals, R. J., Stability characteristics of a single-phase free convection loop. *Journal of Fluid Mechanics*, 1975, **67**(1), 65–84.
2. Ehrhard, P., Karcher, Ch. and Muller, U., Dynamical behavior of natural convection in a double loop system. *Experimental Heat Transfer*, 1989, **2**, 13–26.
3. Davis, S. H. and Roppo, M. N., Coupled Lorenz oscillators. *Physica D*, 1987, **24**, 226–242.
4. Hartmann, J., Hg-dynamics in a homogeneous magnetic field, Part I. *Mathematical Physics Journal, Copenhagen*, 1937, **15**(6).
5. Cramer, K. R. and Pai, S., *Magneto Hydrodynamics for Engineers and Applied Physics*. McGraw-Hill, New York, 1973, Chapter 4, p. 114.